Water–Soluble Extracts from Banana Pseudo–stem as Functional Additives for Polylactic Acid: Thermal and Mechanical Investigations

Thomas Sango, Grégory Stoclet, Nicolas Joly, Adeline Marin, Arnaud Maxime Cheumani Yona, Lucie Duchatel-Crepy, Maurice Kor Ndikontar, Jean Marc Lefebvre

Water–Soluble Extracts from Banana Pseudo–stem as Functional Additives for Polylactic Acid: Thermal and Mechanical Investigations

Thomas Sango[a,b], Gregory Stoclet[a], Nicolas Joly [c,*], Adeline Marin[a], Arnaud M. Cheumani Yona[b], Lucie Duchatel[d], Maurice Kor Ndikontar[b], Jean–Marc Lefebvre[a]

[a] Unité Matériaux Et Transformations (UMET), UMR CNRS 8207, Université de Lille, Sciences et Technologies, 59655 Villeneuve d'Ascq, France

[b] Unité de Chimie Macromoléculaire, Laboratoire de Chimie Inorganique Appliquée (LCIA), Département de Chimie Inorganique, Faculté des Sciences, Université de Yaoundé 1, BP 812 Yaoundé, Cameroun

[c] Univ. Artois, UnilaSalle, Unité Transformation & Agroressources, EA7519, IUT de Béthune, F–62408, Béthune cedex, France

[d] Univ. Artois, EA 4515, Laboratoire de Génie Civil et géo–Environment (LGCgE), F–62400, Béthune, France

ABSTRACT: Water–Soluble Extracts (WSE) were obtained from Banana Pseudo–stems (BPS) using a simple and robust deconstruction procedure. WSE were characterized by FTIR, WAXS, TGA–DTG analysis. With the objective of developing fully bio–based polymer formulations, WSE fillers were blended to Poly Lactic Acid (PLA) using a solution blending, casting and thermocompression process. Thermal and mechanical properties were investigated by Differential Scanning Calorimetry (DSC), Dynamic Mechanical Analysis (DMA) and uniaxial tensile tests on neat–PLA (n–PLA) and PLA/WSE blends at various filler contents. Thermal DSC investigations established that WSE act as a plasticizer on PLA. This was further confirmed by DMA by the shift of the loss factor (tan δ) peak maximum

towards lower temperatures. WSE also significantly impacted the thermally induced crystallization of PLA and the nucleating power of WSE was assessed by isothermal and non–isothermal studies. WSE had a detrimental effect on PLA brittleness and a slightly positive influence on its stiffness in the glassy state, whereas the drawability remained fairly acceptable when PLA–based materials where drawn at 75°C above T_g. Moreover, WSE induced an earlier strain–hardening of the composite films as compared to neat PLA. These results underline the valorization potential of such agricultural by–products for sustainable polymer applications in the packaging industry.

Keywords: *Poly(lactic acid), Banana pseudo–stem, Water Soluble Extracts, Polymer plasticization, Crystal nucleation, Thermo–mechanical properties.*

1. Introduction

Polymer–based materials are versatile materials that have found applications in almost all the sectors of society world–wide. They however yield a significant amount of waste, which raises serious disposal issues [1]. As a consequence, environmental concerns associated to the non–biodegradability of conventional petro–sourced polymer materials have led to an increasing need for sustainable alternatives, such as bio–based polymers and composites [1,2]. Bio–based composites, typically consisting of a combination of bio–fillers and bioplastic polymers, may provide such alternatives in terms of both recyclability and biodegradability [2]. For instance, compostable materials may be easily disposable at the end of service life through a series of biodegradations by living organisms [3]. In this context, Polylactic acid (PLA) is the most extensively studied and industrialized biopolymer. It is a renewable aliphatic thermoplastic polyester obtained through direct condensation polymerization of lactic acid (2–hydroxy propionic acid) or by ring–opening polymerization (ROP) of an intermediate lactide, the cyclic dimer of lactic acid [4]. These monomers can be obtained by

microbial fermentation of carbohydrate–rich agricultural by–products [5] or industrially produced through biorefining of sugars and polysaccharides such as starch [4,6]. PLA is bio–resorbable, bio–compostable, and thus biodegradable under controlled composting conditions [2,7]. It is widely considered as a potential environmentally friendly substitute for petro–sourced polymers like polyethylene terephthalate (PET) which causes environmental pollution [8,9]. Even though it is costly [2,10], PLA is currently commercialized and used in flexible and rigid food packaging applications for fresh or relatively short shelf–life products and as containers, drinking cups, salad cups, blister packages, overwrap and lamination films [3,11]. The most advanced applications include drug delivery systems, healing products and surgical implant devices, orthopaedic devices, bio–resorbable scaffolds for tissue engineering and others pharmaceutical furnishings like internal sutures, scaffolds and implant cell carriers [3,6,8]. PLA however suffers from some shortcomings such as low–ductility and toughness as well as low crystallization rate [4,8].

From a general point of view, a polymer material is formulated with different kind of additives, such as plasticizers, antimicrobial substances, Ultra–Violet (UV) stabilizers, flame retardants, pigments and other fillers, in order to enhance its physical properties (2,3,12]. In this respect, PLA formulation is considered as a powerful method for obtaining specific end–use characteristics and major property enhancements [4]. Additives may be organic, inorganic, natural or synthetic but the current trend emphasizes the need for more eco–friendly functional fillers [1,3]. As previously noticed by many authors [11,13–17], numerous attempts have been made to improve PLA properties by blending with natural substances such as nucleating agents and plasticizers. Inorganic fillers, such as carbonaceous compounds, hydroxyapatite, barium sulphate, calcium carbonate and β–tricalcium phosphate, ~~carbon nanotubes~~, clays (Talc, Kaolin, Montmorillonite, halloysite, hydroxyapatite), are examples of additives which have also proven to be more or less efficient for enhancing the crystallisation

rate and thermomechanical properties of PLA [4,7,14,16,18–20]. Organic compounds may ~~be good candidates~~ as well positively affect the crystallyzation of PLA [14]. Polymer formulation is typically achieved by adding some low molecular weight substances to the polymer which will crystallize at temperatures higher than the crystallization temperature of PLA and provide nucleation sites [4]. Qi et al. [14] reported that blending PLA with 1% wt aliphatic diacyl adipic dihydrazides can enhance both crystallization rate and crystallinity of PLA. They also mentioned a study comparing the nucleating ability of hydrazide compounds with talc and *N*,*N*–ethylenebis(12–hydroxystearamide) on PLA. Selected hydrazide compounds enabled complete crystallization of PLA upon cooling with a high crystallization enthalpy (ΔH_c = 46J/g), while that of Talc and *N*,*N*–ethylenebis(12–hydroxystearamide) only showed ΔH_c of 26 and 35 J/g respectively under the same conditions. Biocompatible plasticizers like oligomeric lactic acid, glycerol and citrate ester were also added to PLA and the resulting product gained in flexibility, ductility, resilience and crystallinity [4,22]. Various low–cost native and functionalized polysaccharide additives like natural fibres, cellulose particles (cellulose nanocrystals or whiskers, micro–fibrillated cellulose,...), hemicelluloses (xylans) and lignin, were also blended with PLA and proved their effectiveness for enhancing the crystallization rate and thermomechanical properties of the neat biopolymer [1,11,13,23,24]. Besides those polysaccharide fillers which are the main components of the plant cell wall, there are some other parietal substances like plant extractives that may be blended with PLA [25].

Extractives are non–structural plant sub–components and usually represent a minor fraction of plant composition [26]. They are necessary to maintain diverse biological functions of the plant like protection against microbiological damage or insect attack. They can be found in various parts of plants (stem, branches, roots, bark and needles). Their content and composition widely vary according to species and even growth conditions. ~~They are bioactive~~

Extractive ~~substances,~~ are generally subdivided into ~~green~~ lipophilic (organic–soluble) and hydrophilic (water–soluble) extracts [27,28]. In agricultural by–products, organo–soluble extracts are mostly composed of fatty acids (palmitic, stearic, linoleic, 22–hydroxydocosanoic, 24–hydroxytetracosanoic~~…~~), sterols (campesterol, stigmasterol and sitosterol) and others such as aromatic compounds, fatty alcohols and alkanes [27]. On the other hand, water–soluble extracts (WSE) of the same bio–resources are composed mainly of sugars, phenolics (hydrolyzable tannins) and ash [28]. In sub–tropical countries such as Cameroon, aqueous decoctions of fresh banana pseudo stems are used locally as traditional crude drugs to treat various diseases. In fact, many plant extracts have specific biological and pharmacological activities, (antimicrobial, antitumor, antifungal, antioxidant~~…~~) [29–32]. They can be used in ~~such~~ fields such as cosmetics, food processing, biomedical, wood preservation, dyeing and adhesives [32,33]. Millions of tons of ecophilic extracts of tropical heartwoods are produced annually and used to colour wine, food, synthetic and vegetable fibers. Phenolic substances and carbohydrates, easily soluble in water, are already exploited in ~~industry~~ the pharmacopeia. ~~One of the well–known examples is the~~ Hydrolysable ~~oak~~ Moabi and Movingui tannins ~~well known~~ are used for their antioxidant, anti–rheumatism, anti–tumor, ~~antiseptic~~, ~~anti–cancer and~~ cardiovascular disease prevention properties and for fighting dermatitis [32,33].

The incorporation of naturally occurring phenolics (α–tocopherol, resveratrol, and quercetin) as well as plant extracts in polymer formulations, intended for active packaging applications, has been reported only recently and their stabilizing effect has been assessed [1,12]. Several studies have shown that polyphenols present in agro–industrial wastes, such as spent coffee grounds, grape pomace and lignins, elicit a powerful stabilizing action on some polymer materials which can be useful in food packaging since their antioxidant activity can restrain the putrefaction of packed foodstuffs. Alippilakkotte et al. [34] reported that a composite of

PLA and silver (Ag) ~~PLA/Ag~~ nanofibers, mixed with water–soluble *Momordica charantia* fruit extracts, has shown an antimicrobial activity for wound dressing. Even though several studies in this domain used rather expensive plant extracts or even pure compounds, Saha and co–workers [33] have shown that alkaline and aqueous extracts of Padouk and Movingui sawdusts can be used as dyes on cotton fabric, wood viscose and bamboo viscose textiles. Thus, using natural bio–waste extracts as bio–additive source for reinforcing polymers is an attractive opportunity.

In the present work, the incorporation of Water–Soluble Extracts (WSE) obtained from Banana Pseudo–stems (BPS) into Polylactic Acid (PLA) has been investigated. In a first step, WSE were isolated and characterized by Wide Angle X–ray Scattering (WAXS), Fourier Transform Infra–Red spectroscopy (FTIR), Differential Scanning Calorimetry (DSC) and Thermogravimetric Analysis (TGA–DTG). In a second step, PLA/WSE materials of varying compositions were prepared using a solution casting–thermocompression method and the impact of WSE additives on the thermal and mechanical behavior of PLA was investigated with a specific focus on thermal behavior, polymer crystallization and uni–axial tensile response.

2. Experimental section

2.1. Materials

The materials used in this study included PLA (commercial grade 4042D purchased from NatureWorks–USA), containing 4.3% mol of D–isomer units with a polydispersity index I_p=1.62 (number– and weight–average molar masses M_n = 116kDa; M_w = 188kDa, respectively). BPS from *Musa acuminata* species, graciously provided by the Cameroon Development Corporation (CDC, Tiko, Bota–Limbe, South–West Region/Cameroon), were randomly selected and freshly cut–off from the mature plants directly after fruit bunches were

harvested. Ethanol, toluene, chloroform and deionized water were purchased from Verbiese (France) and used without further purification.

2.2. Isolation of WSE from BPS

The overlapped petiole sheath leaves of banana pseudo–stems were handily separated from each other, cleaned, sun–dried during three weeks and cut into 0.5*0.5 cm^2 pieces. These chunks were ground to pass a through 1.0 mm size sieve (Fig. 1).

Fig. 1. Preparation of ~~BPS~~ banana pseudo–stem sample.

WSE were recovered in the second stage of the step–wise deconstruction process of BPS described elsewhere [25]. An initial mass (m_i) of powder, dried overnight in a vacuum oven at 70°C, was then defatted in a toluene–ethanol (2:1, v/v) mixture in a Soxhlet extractor for 8h at 80°C. The residue was dried in vacuum oven at 70°C for 2h in order to remove all traces of solvents. Then, a precise mass of the dried sample, free from lipophilic extracts (LE), was then soaked in deionized water and stirred ~~(step 1)~~. The decoction was refluxed for 2h at 90°C ~~(step 2)~~. The hot suspension was filtered ~~(step 3)~~, the filtrate was concentrated under vacuum ~~(step 4)~~, refrigerated ~~(step 5)~~, freeze–dried ~~(step 6)~~ and the resulting WSE were weighed (m_f) and directly ~~dark~~ kept in the dark an oven at 40°C in order to avoid the adsorption of water molecules contained in the ambient moisture ~~(see Fig. 2)~~. The extraction yield (Y_{ex}) was calculated as mass percentage of the initial dried BPS using Eq. (1).

~~**Fig. 2.** Succinct steps for recovering WSE.~~

~~The extraction yield (Y_{ex}) was then calculated using Eq. (1):~~

$$~~Y_{ex} = \frac{m_f}{m_i} \times 100~~ \qquad ~~(1)~~$$

2.3. Preparation of ~~PLA/WSE~~ PLA–based blends

PLA–based films were prepared using a solution casting–thermocompression method. Depending on the targeted formulation in the blended products ~~(Table 1)~~, the desired amount of anhydrous WSE was dispersed in 50 mL of chloroform ($CHCl_3$). The corresponding amount of dried PLA was added and the mixture was stirred until complete dissolution of PLA. Each visquous solution was poured into levered glass petri dishes and the solvent was allowed to evaporate at room temperature (RT), 30°C average. The dishes were covered in order to enable slow casting and prevent dust contamination of ~~the~~ films. ~~Table 1 shows the formulations of the different~~ Different formulations of PLA/WSE ***x*** composite materials were prepared. ~~where~~ Here, ***x*** (2; 10; 20; 30) is the percentage of WSE portion in the composite. For comparison, a neat PLA (n–PLA) reference film was also produced using the same procedure described above at ***x*** = 0.

~~**Table 1** Compositions of the different PLA/WSE formulations~~

~~Material designation~~	~~Mass of PLA (g)~~	~~Mass of WSE (g)~~
~~n–PLA~~	~~3.00~~	~~0~~
~~PLA/WSE 2~~	~~2.94~~	~~0.06~~
~~PLA/WSE 10~~	~~2.70~~	~~0.30~~
~~PLA/WSE 20~~	~~2.40~~	~~0.60~~
~~PLA/WSE 30~~	~~2.10~~	~~0.90~~

All films were removed from petri–dishes after drying, further dried in a vacuum oven at 180°C for 3 min in order to remove residual $CHCl_3$ and thermo–compressed (50 bars) at 180°C for 2 min. The resulting films were amorphous sheets of ca. 200 µm thickness.

2.4. Characterization of materials

2.4.1. ~~ATR–FTIR~~ Fourier Transformed Infra–red analysis

Fourier Transformed Infrared (FTIR) ~~FTIR~~ analyses were performed using an *Agilent Cary 630* apparatus equipped with a diamond crystal operated in ATR mode. The infrared spectrum was recorded from 600 to 4000 cm^{-1} by accumulation of 32 scans with a resolution of 4 cm^{-1}. All samples were dried under vacuum at 80°C for 12 h before testing.

2.4.2. Wide Angle X–ray Scattering ~~Structural~~ analysis

Wide–Angle X–ray Scattering (WAXS) analyses were carried out using a Genix micro–source equipment (Xenocs, France) operating at 50 kV and 1 mA. The Cu Kα radiation used (λ = 1.54 Å) was selected with a curved mirror monochromator (Fox2D–12Inf, Xenocs). WAXS patterns were recorded on a 2D CCD VHR camera (Photonic science), the distance between sample and detector (D) being set at 7cm for WAXS. The working distance was calibrated using silver behenate as standard. Standard corrections such as distortion, dark current subtraction and background correction were applied before analysis. Experiments were conducted at RT in transmission mode in the 5°–35° 2θ range.

2.4.3. ~~Non–isothermal~~ Differential Scanning Calorimetry (DSC) analyses ~~measurements~~

Non–isothermal DSC measurements: Thermal transitions of PLA and its biocomposites were investigated using a DSC Q20 apparatus from TA Instruments. For each run, samples of mass lower than 18mg were inserted into hermetically sealed aluminium pans and scanned from RT to 200°C, held for 5min to erase the previous thermal history, then cooled to 30°C at a rate of 10°C.min^{-1}, and finally heated again to 200°C at the same rate under nitrogen (N_2) flow. The apparatus was calibrated using indium according to standard procedures. From these

thermograms, glass transition temperature at midpoint (T_g), heat–capacity increment (ΔC_p), cold crystallization temperature (T_{cc}), melting temperature (T_m), heat of cold crystallization (ΔH_m), heat of melting (ΔH_m) and the degree of crystallinity within the PLA fraction (χ_c) were determined. The data presented here were recorded and determined from the second heating scan. The degree of crystallinity was calculated using Eq. (1):

$$\chi_c = \frac{\Delta H_m}{w \Delta H_m^0} \times 100 \quad (1)$$

where ΔH_m^0 = 93 J/g is the standard melting enthalpy corresponding to perfect PLA α–crystals and w is the mass fraction of PLA in the biocomposite [35].

~~*2.4.4. Isothermal DSC measurements*~~

Isothermal DSC measurements: Each dried sample (5–18 mg) was scanned from RT to 180°C at a heating rate of 40°C.min^{-1}, held for 2 min at the latter temperature to ensure complete melting, and then quenched to 120°C (40°C.min^{-1}) and held there for 10, 20, 30 and 40 min to allow crystallization. Afterwards, the sample was brought to RT (40°C.min^{-1}) and then heated from 30 to 180°C at 10°C.min^{-1} in order to determine the amount of crystals formed.

2.4.4.~~5~~. ~~TGA DTG~~ Thermogravimetric analysis

Thermogravimetric analyses were performed on a TGA Q500 thermal gravimetric analyzer (TA Instruments). 5–10 mg of WSE were heated from 30 to 700°C at a heating rate of 10°C.min^{-1} using a porcelain crucible pan under N_2 flow (50 mL.min^{-1}).

2.4.5.~~6.~~ Tensile testing

Uniaxial deformation tests of composite films were performed as a function of temperature on an Instron Testing Model 4466 equipped with a temperature controlled oven. The dumbbell–

shaped specimens (initial gauge length, L_0 = 15 mm; width, l_0 = 4 mm, thickness, e_0) were strained at a constant cross–head speed of 10 mm.min^{-1}, *i.e.* an initial strain rate $\dot{\varepsilon} = 1.1 \times 10^{-2} s^{-1}$ at 40°C (below T_g) and 75°C (above T_g) respectively using a load cell of 100 N. Each specimen was held at test temperature for 3 min in order to stabilize the temperature prior to testing. At least four specimens per formulation were tested to ensure reproducibility. The nominal or engineering stress σ and strain ε were computed conventionally using Eq. (2) and (3):

$$\boldsymbol{\sigma = \frac{F}{S_0}} \qquad \textbf{(2)}$$

$$\boldsymbol{\varepsilon = \frac{L - L_0}{L_0} \times 100} \qquad \textbf{(3)}$$

where F is the applied force, $S_0 = l_0 \times e_0$ is initial sample cross–section and L is the gauge length of the sample during deformation.

2.4.6.~~7.~~ ~~DMA~~ Dynamic Mechanical Analysis measurements

DMA experiments were carried–out in a tensile mode using a TA Instruments RSA3 apparatus operating at a frequency of 1 Hz under dry air flow. Parallelepipedic specimens (length 50 mm; width 4 mm; thickness calculated from an average of three measurements) were cut from the film. Heating scans were conducted in the temperature range 30–95°C at the heat speed of 5°C.min^{-1}.

3. Results and discussion

3.1. WSE characterizations

3.1.1. Yield of extraction with water

From an initial mass of 30 g of the lipophilic extract–free raw material, an average mass of 3.7 g of dried WSE was recovered for an average of three replicates [25]. This corresponds to an extraction yield of 12 ± 2%. This yield is higher compared to the 9% obtained by Oliviera et al. [28] on a BPS sample of a Musa acuminata species from Portugal ~~the same Portuguese species~~. The chemical compositions of a plant species vary generally form one to another due to factors like soil composition and climate [26]. These values are relatively high when compared to wood species such as Moabi: 8.4 ± 0.3%, Movingui: 3.8 ± 0.1%, Padouk: 4.0 ± 0.1% and Tali: 10.0 ± 0.2% [32] or to some other plants [36–38]. A chemical screening of BPS leaf sheaths from *Musa acuminata* extractives carried–out by Oliviera et al. [28] showed that WSE were composed of 33.3% of carbohydrates (mostly glucose), 17.5% of other organic substances (uronic acids and hydrolysable tannins) and 49.2% of ash.

3.1.2. Fourier Transformed Infra–red ~~ATR–FTIR~~ analysis of WSE

Extracts of a lignocellulosic material are complex mixtures of various compounds difficult to be fully described chemically [27,28]. FTIR, done in Attenuated Total Reflectance (ATR) mode, was used to obtain primary information on the chemical composition through the various functional groups revealed. ATR–FTIR spectrum of WSE is shown in Fig. 2 ~~3~~.

Fig. 2 ~~3~~. ~~FTIR–ATR~~ Fourier Transformed Infrared absorption spectrum of WSE.

The spectroscopic signature is quite similar to the one reported by Oliviera et al. [28] for extracts of BPS leaf sheaths from a *Musa acuminata* species harvested in Portugal. The broad intense band at 3268 cm^{-1} was attributed to the stretching of hydroxyl $(O-H)$ groups

[27,28]. The band at 2926 cm^{-1} can be assigned to symmetric and asymmetric stretching of various $C-H$ bonds in methylene and methyl groups. The band at 1592 cm^{-1} was attributed to the stretching vibration of conjugated $C=C$ groups generally found in phenolic compounds [25]. The intensity of this band indicates that the extract contains a high proportion of phenolic compounds, probably condensed or hydrolysable tannins [39].

The band at 1312 cm^{-1} corresponds to $C-H$ in plane bending and conjugated $C-O$ stretching. The presence of bending and twisting frequencies of phenols and $C-O-C$ glycosidic linkage vibrations, detected from 1200 to 1002 cm^{-1} may be related to the presence of low molecular weight circulating sugars that were dissolved by water [27,28,39].

3.1.3. Structural and thermal characterizations of WSE

Fig. 3 a shows the 1D–WAXS patterns of dried WSE sample.

Fig. 3 a. 1D–Wide Angle X–ray Scattering patterns ~~1D–WAXS~~ of WSE; **b.** First and second scan Differential Scanning Calorimetry ~~DSC~~ curves of WSE; **c.** Thermogravimetric ~~TGA–DTG~~ curves of WSE.

The diffractogram shows an intense peak observed at 2θ = 28° and a smaller one around 6°. This confirms the presence of an ordered phase in the raw WSE sample that could be either an organic or an inorganic phase. Guimarães et al. [39] additionally reported with banana fibres, the presence of narrow scattering low intensity peaks that they attributed to unknown contamination from inorganic substances. In the present case, it is difficult to assess the presence of such peaks in the very blurry background.

Typical first and second heating DSC scans on WSE are presented in Fig. 3b. The tests were carried out four times and the results proved to be reproducible, similar thermograms were obtained from these different tests. During the first heating, the thermogram revealed a heat

capacity jump (glass transition), around 43°C, followed by a broad endotherm culminating in the temperature range 130–140°C. A weak endothermic transition was also observed at the latter temperature location during the second heating, whereas the broad endotherm had vanished. It is therefore reasonable to postulate that the broad endotherm of the first scan comprises both a major contribution linked to water desorption (considering the hydrophilic nature of the compounds with a proportion of structurally bound water) and a narrow melting endotherm of a crystallized WSE component in relation to the scattering peak observed in WAXS (Fig. 3a). The enthalpy drop from ΔH_m = 130.7 J/g during the first scan, (where melting of partially crystallized WSE is merged in the contribution of water departure), down to ΔH_m = 0.2 J/g during the second scan is also indicative of the fact that the melted crystallized component was not able to recrystallize properly under the imposed cooling conditions. The glass transition phenomenon at 43°C may be associated to a change in the molecular dynamics of some WSE components present in sugars or uronic moieties. Crépy et al. [40] suggested that the origin of this molecular motion may be assigned to a boat–chair configuration change of the glucose ring and/or to local motion of the aliphatic chains (uronic moieties) which are unlocked at 43°C. It is also worth noting that the temperature range of the DSC endotherm does not favour the fusion of inorganic compounds and therefore the WAXS diffraction pattern and DSC data point at the presence of crystallized organic matter in water soluble extractives.

TGA–DTG curves of WSE, shown on Fig. 3c, exhibit four main mass loss steps. The first mass loss, of approx. 4% occurs below 130°C and is attributed to water desorption from the sample, in agreement with the contribution of water loss to the broad endothermic peak observed during the first heating scan in DSC experiments. The low temperature shoulder to the main degradation peak on the DTG curve also points out a degradation event occurring around 200°C. This event may be associated to the degradation of water–soluble small

polymerized sugars or carbohydrates as Gaugler and Grigsby [41] noticed on condensed tannins from Radiata Pine bark. The main peak at 264°C reflects the decomposition of hydrolysable tannins [41]. Between 430 and 530°C, another broad degradation peak is associated to the carbonisation of WSE. Beyond 550°C, only ashes are identified [39], indicating the presence of a significant amount of inorganic salts in WSE, and consequently supporting the assumption of the presence of mineral salts contributing to the background–noisy signal observed in WAXS.

3.2. ~~PLA/WSE~~ PLA–based blends characterization

3.2.1. Non–isothermal Differential Scanning Calorimetry ~~DSC~~ analysis of ~~PLA/WSE~~ PLA–based mixtures

As previously stated, WSE were dispersed in a PLA polymer matrix at different loadings using a solution casting method to prepare composite films. DSC thermograms of different films are depicted in Fig. 4 ~~5~~ and key data of the composites are summarized in Table 1~~2~~.

Fig. 4. Differential scanning calorimetry of n–PLA and PLA/WSE blends.

It is quite obvious at first sight that dispersing WSE in PLA has a significant influence on the thermal behaviour of the biopolymer. The cold crystallization temperature decreases from 130°C (for the neat–matrix) to 123°C (for PLA/WSE 30) while the melting enthalpy increases from 1.4 J/g (n–PLA) to 30.4 J/g (PLA/WSE 30), revealing the nucleating effect of WSE which strongly impacts the crystallization kinetics of the amorphous PLA matrix. In fact, one may assume that the presence of crystallized WSE particles in contact with PLA macromolecules promotes crystal nucleation, as Agustin–Salazar et al. [1] noticed with nutshell extracts in the same polymer matrix.

Table 1. Differential Scanning Calorimetry ~~DSC~~ data of ~~PLA/WSE~~ PLA–based materials (T_g: glass transition temperature at midpoint in °C; ΔC_p: heat–capacity increment in $J.g^{-1}.K^{-1}$; T_{CC}: cold crystallization temperature in °C; T_m: melting temperature in °C; ΔH_{CC}: heat of cold crystallization in $J.g^{-1}$; ΔH_m: heat of melting in $J.g^{-1}$; χ_c: degree of crystallinity in %).

Sample	T_g (°C)	ΔC_p ($J.g^{-1}.K^{-1}$)	T_{CC} (°C)	ΔH_{CC} ($J.g^{-1}$)	T_m (°C)	ΔH_m ($J.g^{-1}$)	χ_C (%)
n–PLA	62	0.10	130	1.3	145–160	1.4	1.5
PLA/WSE 2	62	0.11	129	1.4	145–160	1.4	1.6
PLA/WSE 10	60	0.11	129	7.5	144–160	7.7	9.0
PLA/WSE 20	59	0.10	127	21.4	142–160	21.8	29.0
PLA/WSE 30	58	0.11	123	29.0	138–160	30.4	46.2

The glass transition temperature data presented in Table 1 reveal a 7% drop between neat–PLA (62°C) and PLA/WSE 30 (58°C) indicative of a slight plasticization of PLA as the WSE content is increased. The specific WSE species responsible for this phenomenon are not identified. Further studies including fractionation of the WSE and isolation of some major components of the extract would be required to address this point but this would be out of the scope of a study that aims at valorizing BPS sub–components without having recourse to sophisticated and costly deconstruction processes.

Additionally, plasticizing components of WSE may promote crystallinity due to enhanced PLA chain mobility [22]. The presence of a double melting peak is a well known ~~well–known~~ phenomenon in the case of PLA, ascribed to a melting–recrystallization–melting process. Less perfect crystals (α'–form crystals) are formed at low crystallization temperatures. These crystals have a lower melting temperature than the α crystals formed at higher temperature

which exhibit a higher structural perfection. Thus, when melted the α' crystals have enough time to melt and reorganize into more stable α crystals before they re–melt at higher temperature generating this double peak shape [5,6,10,19,20,23].

The marked evolution as a function of WSE content is in favor of a good dispersion of the latter component, promoting favorable interfacial interactions between the WSE ordered species and PLA that may include the formation of hydrogen bonds network between PLA $C = O$ groups and WSE $O - H$ [17,23,35]. This phenomenon was also observed by Gupta et al. [43] on PLA composites incorporating lignin–coated cellulose nanocrystals.

3.2.2. Isothermal Differential Scanning Calorimetry ~~DSC~~ analysis of ~~PLA/WSE~~ PLA–based mixtures

In order to provide a more quantitative view of the nucleating capability of WSE, isothermal crystallization kinetics were investigated. Fig. 5 reports the isothermal crystallization kinetics at T_c = 120°C of all PLA–based samples.

Fig. 5 . Crystallization kinetics of ~~PLA/WSE~~ PLA–based films at T_c = 120°C.

n–PLA and PLA/WSE 2 exhibit the same slow crystallization kinetics with a crystallization onset after 10 min and a very partial achievement after 40 min. In the case of PLA/WSE formulations with higher loadings, isothermal crystallization starts in the first early seconds of the heating sequence and the process is by far much faster since crystallization is completed within 20 min. This result clearly evidences the nucleating potential of WSE on the bio–polymer matrix and indicates that the crystallization rate of PLA increases as the available WSE particles surface is increased [6,23,35]. It may reasonably be assumed that the ordered component in WSE acted as nucleation site, thus increasing the crystallization kinetics of PLA.

This ~~ordering~~ behaviour was also noticed by Ouchiar et al. [16] (Supporting Information) on PLA/Talc composites, Barrau et al. [18] on PLA/Carbon nanotubes composites and Pei et al. [24] on PLA/silylated cellulose nanocrystals.

3.2.3. Dynamic Mechanical Analysis of ~~PLA/WSE~~ PLA–based films

The respective evolutions of storage modulus E' and loss factor tan δ as a function of temperature are presented in Fig. ~~7~~6a and ~~7~~6b for n–PLA and PLA/WSE films at various WSE loadings.

Fig. 6. Dynamic Mechanical Analysis ~~DMA~~ thermograms of the **a.** E' *vs* temperature and **b.** tan δ *vs* temperature plots for PLA/WSE mixtures at various WSE content and n–PLA as reference.

Fig. 6a shows that in the brittle glassy region (*i.e.* for T < 45°C), the stiffness of PLA in all samples is not significantly affected by the addition of WSE fillers. In this temperature range, WSE are trapped in frozen PLA macromolecular chains, leading to a binary system where the filler particles has a rather negligible reinforcing impact on the stiffness of the polymer matrix [15,17]. Upon heating above 45°C, the material slightly softens as the amorphous PLA chain motions become gradually cooperative [8,9,15]. This is followed, in the temperature range 50–65°C, by the main mechanical α–relaxation of PLA associated to the viscoelastic manifestation of the glass to rubber transition in all formulations and manifested on the plots by an abrupt drop of the storage modulus due to the softening of those amorphous phases [15,21]. It is interesting to mention that the amplitude of the drop in E' decreases with increasing WSE loading, thus revealing the reinforcing effect of fillers in the rubbery state [35]. Indeed, for T > 65°C, all composite films exhibit higher storage modulus as compared to n–PLA. It is worth noticing the onset of rise of the modulus beyond 85°C for PLA/WSE 20 and PLA/WSE 30, as compared to the other formulations. This rise is linked to the occurrence

of a cold crystallization process in PLA induced by the nucleating effect of WSE during the DMA scan, in agreement with the DSC results [6,7,9,15,19]. This behaviour was also noticed by Lu et al. [2] on PLA blended with distiller's dried grains with solubles.

The effect of WSE on the damping behaviour of PLA is presented in Fig. 6b. The shift towards lower temperatures of the tan δ peak maximum position is in good agreement with the results obtained by DSC on the evolution of T_g that established the plasticizing role of WSE. In the meantime, the area under the tan δ peak, related to the extent of damping or energy dissipation due to the segmental motion of the polymer chains, gradually decreases as the WSE concentration in PLA increases. It may be considered that a reduction in chain mobility in the amorphous regions occurs, due to confinement effect, resulting in the reduction in tan δ peak magnitude [9,10,35,43].

3.2.4. Tensile tests of ~~PLA/WSE~~ PLA–based blends

Mechanical properties of the films were evaluated by means of uniaxial tensile tests. Tests were performed below and above T_g at an initial strain–rate of 1.1 10^{-2} s^{-1}. Elongation at break (ε_r), yield strength (σ_y) and elastic modulus (E) were measured for all film samples.

Drawing behavior below T_g (T_d=40°C). Fig. 7 shows the stress–strain curves of n–PLA and PLA/WSE films drawn at T_d = 40°.

Fig. ~~8~~7. Nominal stress–strain curves of n–PLA and PLA/WSE films T_d = 40°C; $\dot{\varepsilon}$ = 0.01 s^{-1}

It can be observed that, in the glassy domain, the stiffness E (Young modulus) of the composites films increases while the strechability drastically decreases with the addition of WSE (Table 2). The same range of Young modulus was obtained for all the WSE contents investigated.

Table 2 Evolution of Young modulus E (MPa), yield stress σ_y (MPa) and elongation at break ε_r with WSE content at T_d = 40°C

Materials	E (GPa)	σ_y (MPa)	ε_r (%)
n–PLA	1.5 ± 0.3	42 ± 2	230 ± 50
PLA/WSE 2	2.4 ± 0.1	44 ± 2	3.5 ± 0.3
PLA/WSE 10	2.4 ± 0.2	43 ± 2	2.5 ± 0.3
PLA/WSE 20	2.6 ± 0.2	35 ± 2	1.8 ± 0.3
PLA/WSE 30	2.6 ± 0.2	30 ± 2	1.5 ± 0.2

These behaviours agree well with the results reported above in Fig. 6a, confirming the fact that WSE have a rather moderate influence on PLA stiffness in the glassy domain. Amorphous n–PLA developed a significant strechability at T_d = 45°C while PLA/WSE formulations were brittle. The stress at break remained practically constant till a WSE content of 10% compared to the reference polymer matrix, then decreased as the WSE loading is increased. This could be imputed to a limited dispersion of WSE in PLA for higher WSE contents due to formation of agglomerates acting as stress concentration points which are detrimental to mechanical properties [6,7,24,43]. The general behaviour observed are typical of amorphous polymers reinforced with more stiff materials in the glassy domain [21,26,35,44].

Drawing above T_g. Tensile tests of all materials were also carried out at T_d = 75°C with an initial strain–rate of 0.01 s^{-1}. The stress–strain data are reported in Fig. 8.

WSE have a significant influence on PLA behaviour in the rubber domain. All samples exhibit a ductile behaviour except PLA/WSE 30. Addition of WSE has a detrimental effect on the mechanical behavior in this temperature domain. For instance, the elongation at break decreases by 62% for a filler content of 20% wt. n–PLA and PLA/WSE 2 display the same

stress–strain deformation profile up to $\mathcal{E}$ = 3% and both exhibit strain–hardening beyond that particular strain level [45,46]. Fracture nevertheless occurs prematurely at 2% WSE loading.

Fig. 8. Nominal stress–strain curves of n–PLA and PLA/WSE films T_d = 75°C; $\dot{\mathcal{E}}$ = 0.01 s^{-1}.

A comparison of PLA/WSE 10 behavior with that of n–PLA reveals two major differences. Firstly, the higher plateau stress level of the blend at 10% wt WSE loading corroborates their reinforcing effect. Secondly, the presence of WSE involves an earlier occurrence of the strain–hardening phenomenon as compared to n–PLA. In the latter case, the strain–hardening is ascribed to the development of a strong strain–induced chain orientation [17,45,46]. We have nevertheless presently no WAXS evidence for the occurrence of such a phenomenon in the present case. At 20% and 30% WSE content, rupture however occurs prematurely.

4. Conclusions

In this paper, we have shown that properties of PLA can be successfully tuned by adding a fraction of Water Soluble Extracts (WSE). ~~Water Soluble Extracts (WSE)~~ WSE from banana pseudo–stems (BPS) of the *Musa acuminata* species were recovered at a yield of 12 ± 2% (based on dry mass of the raw BPS) using a water decoction method. Characterization of WSE was performed by means of FTIR, WAXS, DSC and ATG–DTG experiments. The results showed ~~These have shown~~ that WSE contain a significant proportion of phenolic compounds mixed with carbohydrates. The identification of a glass transition phenomenon around 43°C points at a change in the molecular dynamics of sugars or uronic moieties and WAXS data are indicative of the presence of an ordered organic phase which affects the thermal and mechanical properties of PLA.

PLA–based composites films containing different amount of WSE were prepared using a $CHCl_3$–casting/thermocompression method. Non–isothermal DSC measurements of the films

revealed the plasticizing and nucleating effects of WSE. A 30% wt WSE decreases the T_g of PLA by 7%, and increases its crystallisation kinetics, reducing the cold crystallization temperature from 130°C (for the neat–matrix) to 123°C (for PLA/WSE 30). This nucleation effect was further confirmed by isothermal crystallization studies at 120°C. The WSE crystallized species might in this respect act as nucleation sites. Regarding the dynamic mechanical response, WSE have a moderate stiffening role in the glassy state. Beyond the main mechanical α–relaxation PLA, the reinforcing effect is clearly evidenced particularly in the case of PLA/WSE 20 and PLA/WSE 30 together with a rise in E' beyond 85°C in relation to the cold crystallization of amorphous PLA enhanced by the nucleating power of fillers. The mechanical behavior in tension reveals a brittle behavior below T_g and a fairly good level of ductility above T_g at moderate WSE loading. The occurrence of an earlier strain–hardening stage as exemplified for a 10% wt filler content is of particular interest. Its structural origin has yet to be elucidated and in this respect WAXS experiments during in–situ drawing should provide interesting results.

Overall, the present results underline the ability of WSE to ~~improve the thermal and thermomechanical properties~~ tune the crystallization behaviour of the PLA matrix and suggest that WSE extracted according to a simple deconstruction process might be a good candidate for the development of PLA–based composites for the packaging industry.

Acknowledgments

This work was supported by the *European Commission* through the *KITE–Erasmus Mundus Action I–Lot 18 (ACP 2013–2617)* program which provided the financial support for the doctoral mobility of T. Sango at the University of Lille. The authors express their gratitude to the Cameroon Development Corporation for providing banana pseudo–stems. The authors are also grateful to Région Hauts–de–France and European FEDER for their financial support for

the acquisition of the X–Ray and Thermal equipements. The help of Mr. J.–N. Stealens in chemical characterizations is also gratefully acknowledged.

References

[1] S. Agustin–Salazar, N. Gamez–Meza, L.Á. Medina–Juárez, M. Malinconico, P.Cerruti, Stabilization of polylactic acid and polyethylene with nutshell extract: efficiency assessment and economic evaluation. ACS Sustainable Chem. Eng. 5 (2017) 4607–4618.

[2] H. Lu, S.A. Madbouly, J.A. Schrader, G. Srinivasan, K.G. McCabe, D. Grewell, M.R. Kessler, W.R. Graves, Biodegradation behavior of poly(lactic acid) (PLA)/Distiller's dried grains with solubles (DDGS) composites. ACS Sustainable Chem. Eng. 2 (2014) 2699–2706.

[3] C. Ingrao, C. Tricase, A. Cholewa–Wójcik, A. Kawecka, R. Rana, V. Siracusa, Polylactic acid trays for fresh–food packaging: A carbon footprint assessment. Sci. Total Env. 537 (2015) 385–398.

[4] M. Murariu, P. Dubois, PLA composites: from production to properties. Adv. Drug Del. Rev. 107 (2016) 17–46.

[5] K.M. Nampoothiri, N.R. Nair, R.P. John, An overview of the recent developments in polylactide (PLA) research. Bioresour. Tech. 101 (2010) 8493–8501.

[6] B. Tyler, D. Gullotti, A. Mangraviti, T. Utsuki, H. Brem, Polylactic acid (PLA) controlled delivery carriers for biomedical applications. Adv. Drug Del. Rev. 107 (2016) 163–175.

[7] A.N. Nakagaito, A. Fujimura, T. Sakai, Y. Hama, H.Yano, Production of microfibrillated cellulose (MFC)–reinforced polylactic acid (PLA) nanocomposites from sheets obtained by a papermaking–like process. Compos. Sci. Tech. 69 (2009) 1293–1297.

[8] R.M. Rasal, A.V. Janorkar, D.E. Hirt, Poly(lactic acid) modifications. Prog. Polym. Sci. 35 (2010**)** 338–356.

[9] S. Xu, J. Chen, B. Wang, Y. Yang, Sustainable and hydrolysis–free dyeing process for Polylactic Acid using ~~nonaqueous~~ non aqueous medium. ACS Sustainable Chem. Eng. 3 (2015) 1039–1046.

[10] L.–T. Lim, R. Auras, M. Rubino, Processing technologies for poly(lactic acid). Prog. Polym. Sci. 33 (2008**)** 820–852.

[11] E. Fortunati, M. Peltzer, I. Armentano, L. Torre, A. Jimenez, J.M. Kenny, Effects of modified cellulose nanocrystals on the barrier and migration properties of PLA nano–biocomposites. Carbohyd. Polym. 90 (2012~~a~~) 948–956.

[12] C. Gonzalez–Sanchez, A. Martínez–Aguirre, B. Perez–García, J. Martínez–Urreaga, M.U. de la Orden, C. Fonseca–Valero, Use of residual agricultural plastics and cellulose fibers for obtaining sustainable eco–composites prevents waste generation. J. Cle. Prod. 83 (2014) 228–237.

[13] E. Fortunati, I. Armentano, Q. Zhou, A. Iannoni, E. Saino, L.A. Berglund, J.M. Kenny, Multifunctionnal bionanocomposites films of Poly(lactic acid), cellulose nanocrystals and silver nanoparticules. Carbohyd. Polym. 87 (2012b) 1596–1605.

[14] Z. Qi, Y. Yang, Z. Xiong, J. Deng, R. Zhang, J. Zhu, Effect of aliphatic diacyl adipic dihydrazides on the crystallization of poly(lactic acid). J. Appl. Polym. Sci. 132 (2015) 1489–1495.

[15] G. Stoclet, R. Seguela, C. Vanmansart, C. Rochas, J.–M. Lefebvre, WAXS study of the structural reorganization of semi–crystalline polylactide under tensile drawing. Polymer 53 (2012) 519–528.

[16] S. Ouchiar, G. Stoclet, C. Cabaret, V. Gloaguen, Influence of the filler nature on the crystalline structure of polylactide–based nanocomposites: new insights into the nucleating effect. Macromolecules 49 (2016a) 2782–2790.

[17] S. Ouchiar, G. Stoclet, C. Cabaret, A. Addad, V. Gloaguen, Effect of biaxial stretching on thermomechanical properties of polylactide based nanocomposites. Polymer 99 (2016b) 358–367.

[18] S. Barrau, C. Vanmansart, M. Moreau, A. Addad, G. Stoclet, J.–M. Lefebvre, R. Seguela, Crystallization behaviour of carbon nanotube polylactide nanocomposites. Macromolecules 44 (2011) 6496–6502.

[19] D. Battegazzore, S. Bocchini, A. Frache, Crystallization kinetics of poly(lactic acid)–talc composites. eXPRESS Polym. Lett. 10 (2011) 849–858.

[20] J.–M. Raquez, Y. Murena, A.–L. Goffin, Y. Habibi, B. Ruelle, F. DeBuyl, P. Dubois, Surface–modification of cellulose nanowhiskers and their use as nanoreinforcers into polylactide: A sustainably–integrated approach. Compos. Sci. Tech. 72 **(**2012) 544–549.

[21] J.–M. Raquez, Y. Habibi, M. Murariu, P. Dubois, Polylactide (PLA)–based nanocomposites. Prog. Polym. Sci. 38 (2013) 1504–1542.

[22] O. Martin, L. Averous, Poly(lactic acid): plasticization and properties of biodegradable multiphase systems. Polymer 42 (2001) 6209–6219.

[23] S. Saeidlou, M.A. Huneault, H. Li, C.B. Park, Poly(lactic acid) crystallization. Prog. Polym. Sci. 37 (2012) 1657–1677.

[24] A. Pei, Q. Zhou, L.A. Berglund, Functionalized cellulose nanocrystals as biobased nucleation agents in poly(L–lactide) (PLLA)–Crystallization and mechanical property effect. Compos. Sci. Tech. 70 (2010) 815–821.

[25] T. Sango, A.M. Cheumani Yona, L. Duchatel, A. Marin, M.K. Ndikontar, N. Joly, J.–M. Lefebvre, Step–wise multi–scale deconstruction of banana pseudo–stem (*Musa acuminata*) biomass and morpho–mechanical characterization of extracted long fibres for sustainable applications. Ind. Crops Prod. 128 (2018) 657–668.

[26] O. Faruk, A.K. Bledzki, H.–P. Fink, M. Sain, Biocomposites reinforced with natural fibers: 2000–2010. Prog. Polym. Sci. 37 (2012) 1552–1596.

[27] L. Oliveira, C.S.R. Freire, A.J.D. Silvestre, N Cordeiro, I.C. Torres, D. Evtuguin, Chemical composition of different morphological parts from "Dwarf Cavendish" banana plant and their potential as a non–wood renewable source of natural products. Ind. Crops Prod. 23 (2006) 201–211.

[28] L. Oliveira, N. Cordeiro, D.V. Evtuguin I.C. Torres, A.J.D. Silvestre, Chemical composition of different morphological parts from ‘Dwarf Cavendish’ banana plant and their potential as a non–wood renewable source of natural products. Ind. Crops Prod. 26 (2007) 163–172.

[29] M. Al–Moghazy, M.S. Ammar, M.M. Sief, S.R. Mohamed, Evaluation the antimicrobial activity of artemisia and portcula plant extracts in beef burger. Food Sci. Nut. Stu. 1 (2017) 3–42.

[30] D. Liu, P. Yang, Y.–Q. Zhang, Water–soluble extract of Saxifraga stolonifera has anti–tumor effects on Lewis lung carcinoma–bearing mice. Bioorg. Med. Chem. Lett. 26 (2016) 4671–4678.

[31] A.E. Nkengfack, G.A. Azebaze, J.C. Vardamides, Z.T. Fomum, F.R. Van Heerden, A prenylated xanthone from *Allanblackia floribunda*. Phytochemistry 60 (2002) 381–384.

[32] J.–B. Saha Tchinda, D. Abia, S. Dumarçay, P. Gérardin, N.J. Noah, D. Perrin, Antioxidant activities, total phenolic contents and chemical compositions of extracts from four Cameroonian woods: Padouk (*Pterocarpus soyauxii* Taubb), Tali (*Erythrophleum suaveolens*), Moabi (*Baillonella toxisperma*), and Movingui (*Distemonanthus benthamianus*). Ind. Crops Prod. 41 (2013) 71–77.

[33] J.–B. Saha Tchinda, A. Pétrissans, S. Molina, M.K. Ndikontar, S. Mounguengui, S. Dumarcay, P. Gérardin, Study of the feasibility of a natural dye on cellulosic textile supports by red padouk (*Pterocarpus soyauxii*) and yellow movingui (*Distemonanthus benthamianus*) extracts. Ind. Crops Prod. 60 (2014) 291–297.

[34] S. Alippilakkotte, S. Kumar, L. Sreejith, Fabrication of PLA/Ag nanofibers by green synthesis method using Momordica charantia fruit extract for wound dressing applications. Col. Surf. A 529 (2017) 771–782.

[35] A.P. Johari, S. Mohanty, S.K. Kurmvanshi, S.K. Nayak, Influence of different treated cellulose fibers on the mechanical and thermal properties of poly(lactic acid). ACS Sustainable Chem. Eng. 4 (2016) 1619–1629.

[36] Z. Marrakchi, H. Oueslati, M.N. Belgacem, F. Mhenni, E. Mauret, Biocomposites based on polycaprolactone reinforced with alfa fibre mats. Compos. Part A 43 (2012) 742–747.

[37] P.C. Neto, A. Seca, D. Fradinho, M.A. Coimbra, F. Domingues, D. Evtuguin, A. Silvestre, J.A.S. Cavaleiro, Chemical composition and structural features of the macromolecular components of *Hibiscus cannabinus* grown in Portugal. Ind. Crops Prod. 5 (1996) 189–196.

[38] P.C. Neto, A. Seca, A.M. Nunes, M.A. Coimbra, F. Domingues, D. Evtuguin, A. Silvestre, J.A.S. Cavaleiro, Variations in chemical composition and structure of macromolecular components in different morphological regions and maturity stages of *Arundo donax*. Ind. Crops Prod. 6 (1997) 51–58.

[39] J.L. Guimarães, E. Frollini, C.G. da Si.lva, F. Wypych, K.G. Satyanarayana, Characterization of banana, sugarcane bagasse and sponge gourd fibers of Brazil. Ind. Crops Prod. 30 (2009) 407–415.

[40] L. Crépy, V. Miri, N. Joly, P. Martin, J.–M. Lefebvre, Effect of side chain length on structure and thermomechanical properties of fully substituted cellulose fatty esters. Carbohyd. Polym. 83 (2011) 1812–1820.

[41] M. Gaugler, W.J. Grigsby, Thermal degradation of condensed tannins from radiata Pine bark. J. Wood Chem. Tech. 29 (2009) 305−321.

[42] M.A.S. Anwer, H.E. Naguib, A. Celzard, V. Fierro, Comparison of the thermal, dynamic mechanical and morphological properties of PLA–Lignin & PLA–Tannin particulate green composites. Compos. Part B 82 (2015) 92−99.

[43] A. Gupta, W. Simmons, G.T. Schueneman, D. Hylton, E.A. Mintz, Rheological and Thermo–Mechanical Properties of Poly(lactic acid)/Lignin–Coated Cellulose Nanocrystal Composites. ACS Sustainable Chem. Eng. 5 (2017) 1711−1720.

[44] I.S.M.A. Tawakkal, M.J. Cran, S.W. Bigger, Effect of kenaf fibre loading and thymol concentration on the mechanical and thermal properties of PLA/kenaf/thymol composites. Ind. Crops Prod. 61 (2014) 74−83.

[45] G. Stoclet, R. Seguela, J.–M. Lefebvre, S. Elkoun, C. Vanmansart, Strain–induced molecular ordering in polylactide upon uniaxial stretching. Macromolecules 43 (2010) 1488−1498.

[46] M.M. Reddy, S. Vivekanandhan, M. Misra, S.K. Bhatia, A.K. Mohanty, Biobased plastics and bionanocomposites: Current status and future opportunities. Prog. Polym. Sci. 38 (2013) 1653−1689.

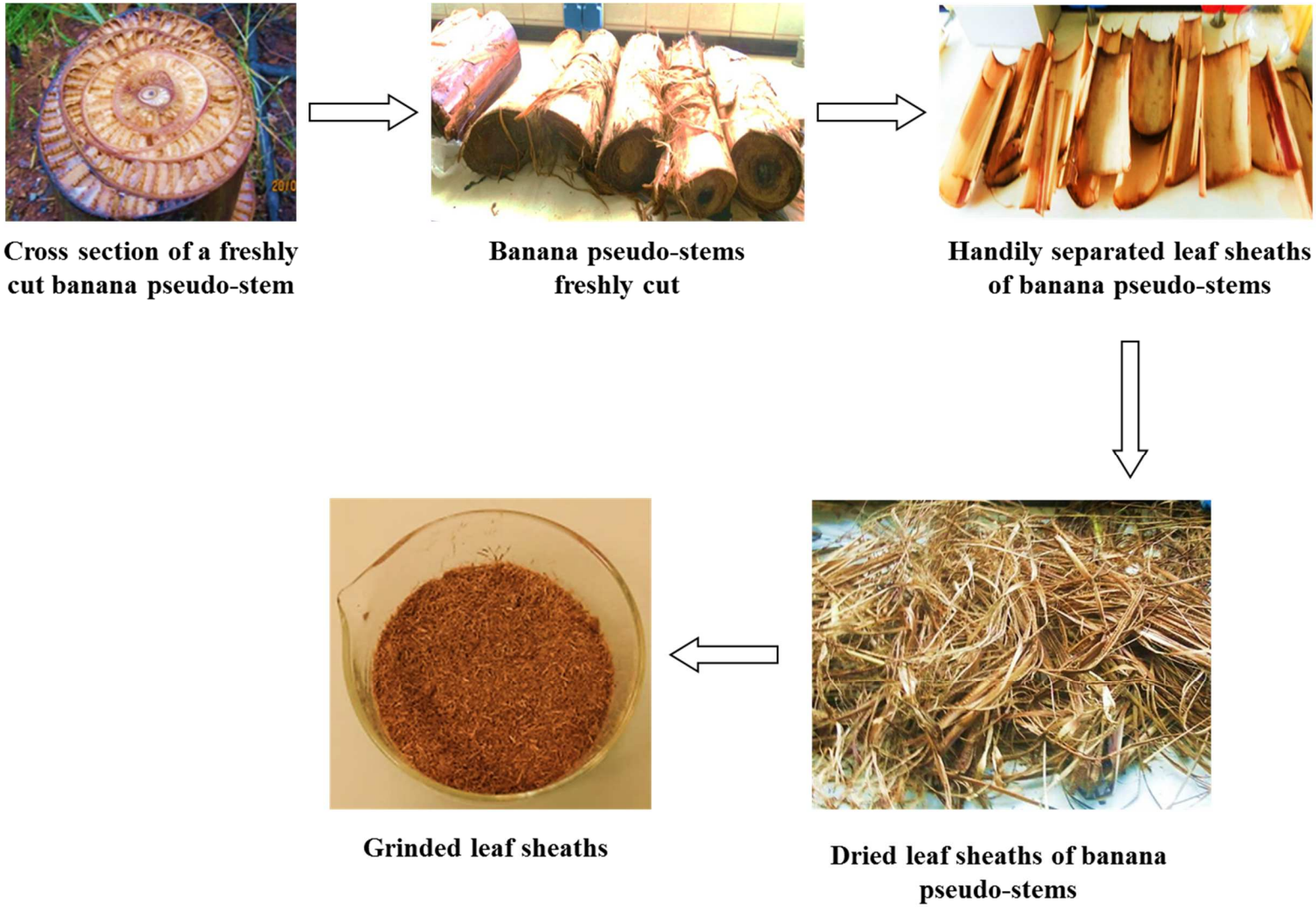

Fig. 1. Preparation of ~~BPS~~ banana pseudo–stem sample.

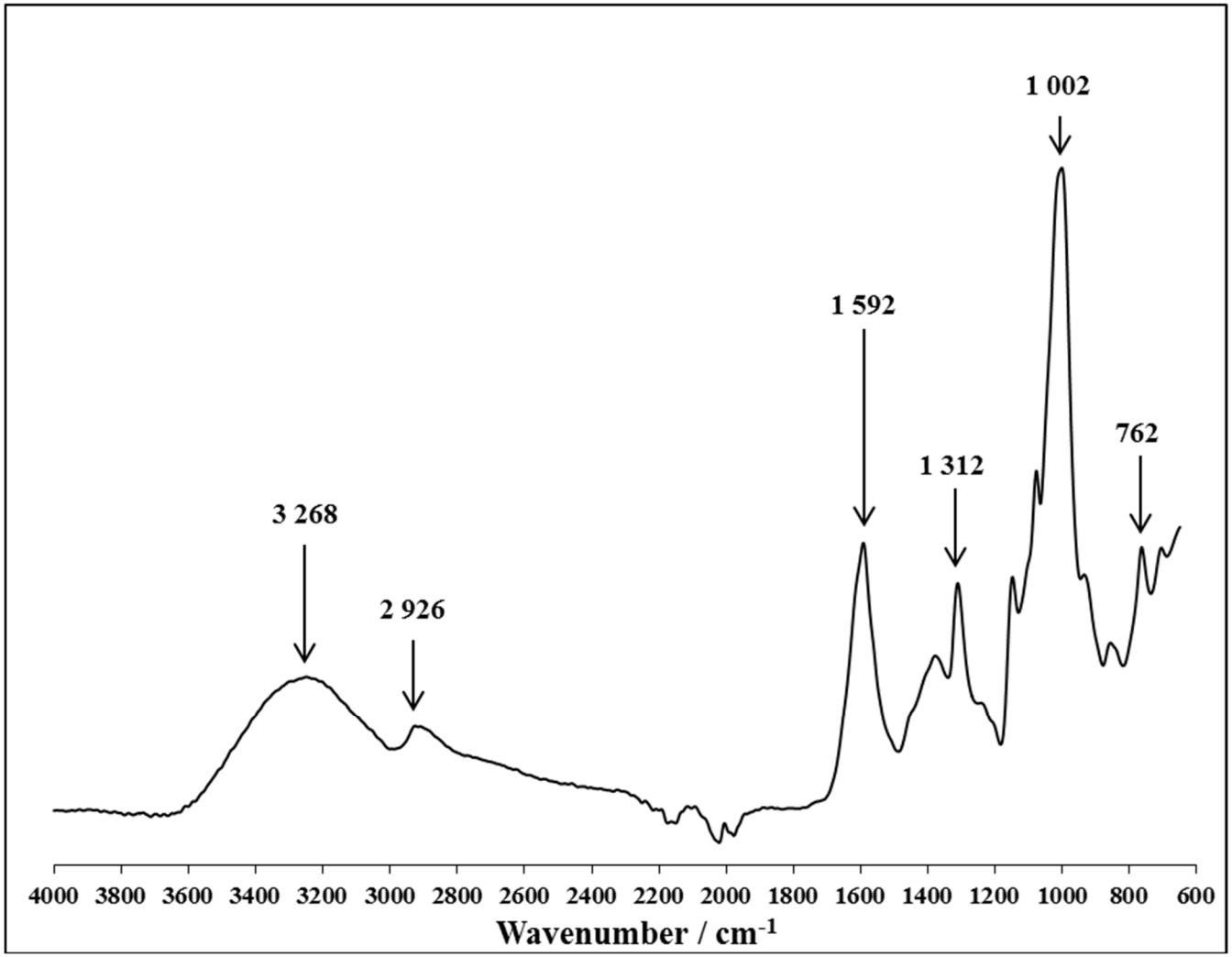

Fig. 3. Fig. 2 ~~3~~. ~~FTIR–ATR~~ Fourier Transformed Infra–red absorption spectrum of WSE.

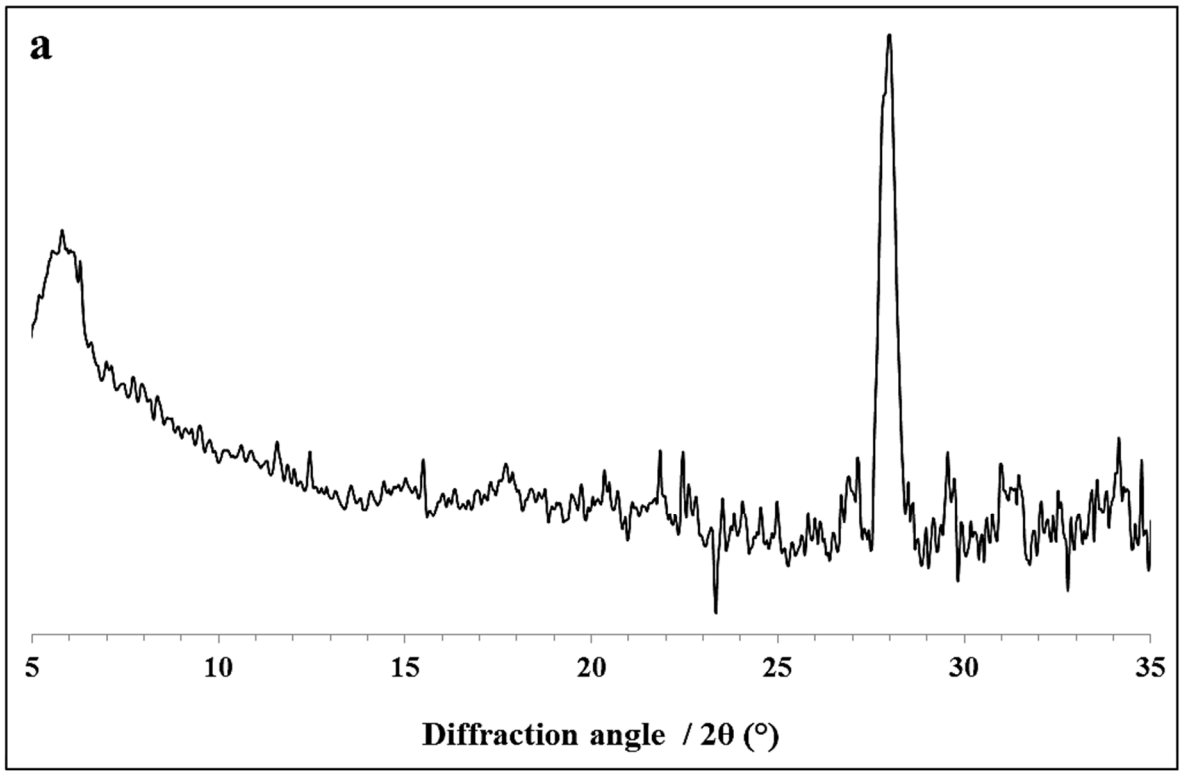
a
5
10
15
20
25
30
35
Diffraction angle / 2θ (°)

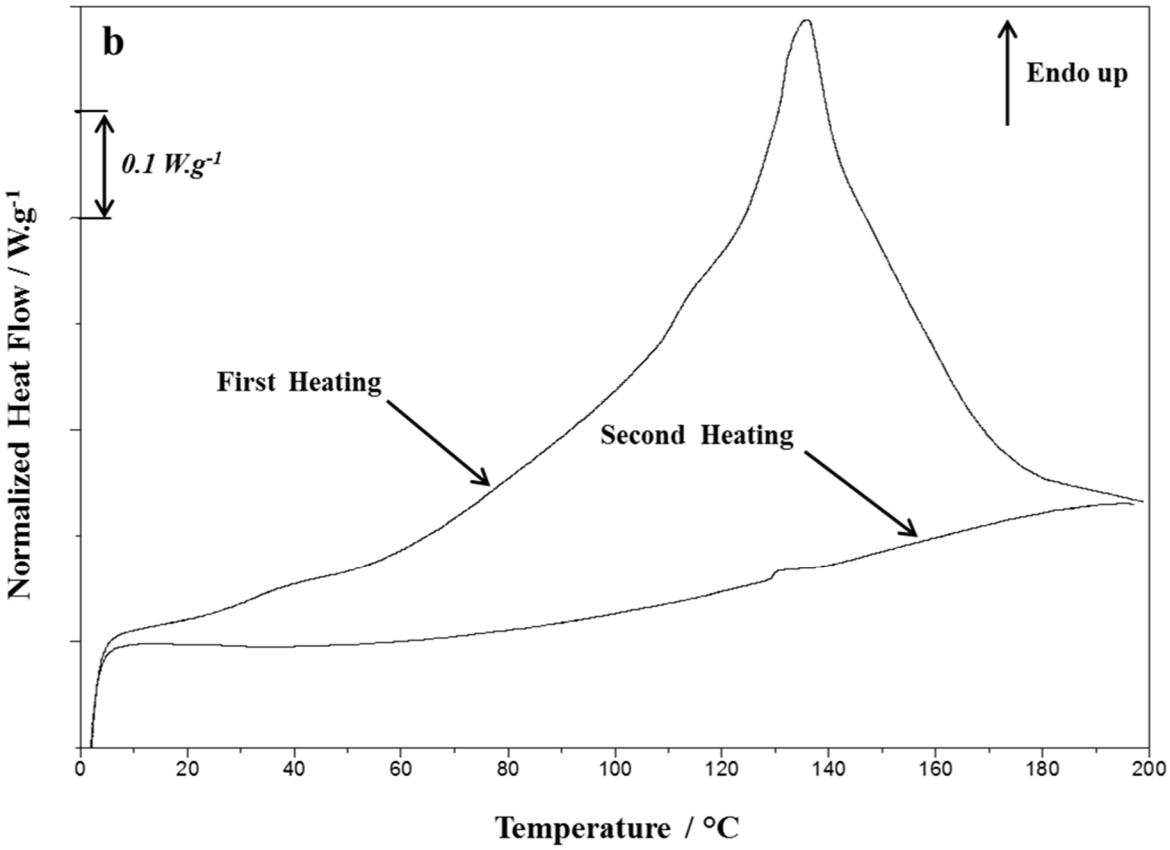
b
Endo up
0.1 W.g-1
Normalized Heat Flow / W.g-1
First Heating
Second Heating
0
20
40
60
80
100
120
140
160
180
200
Temperature / °C

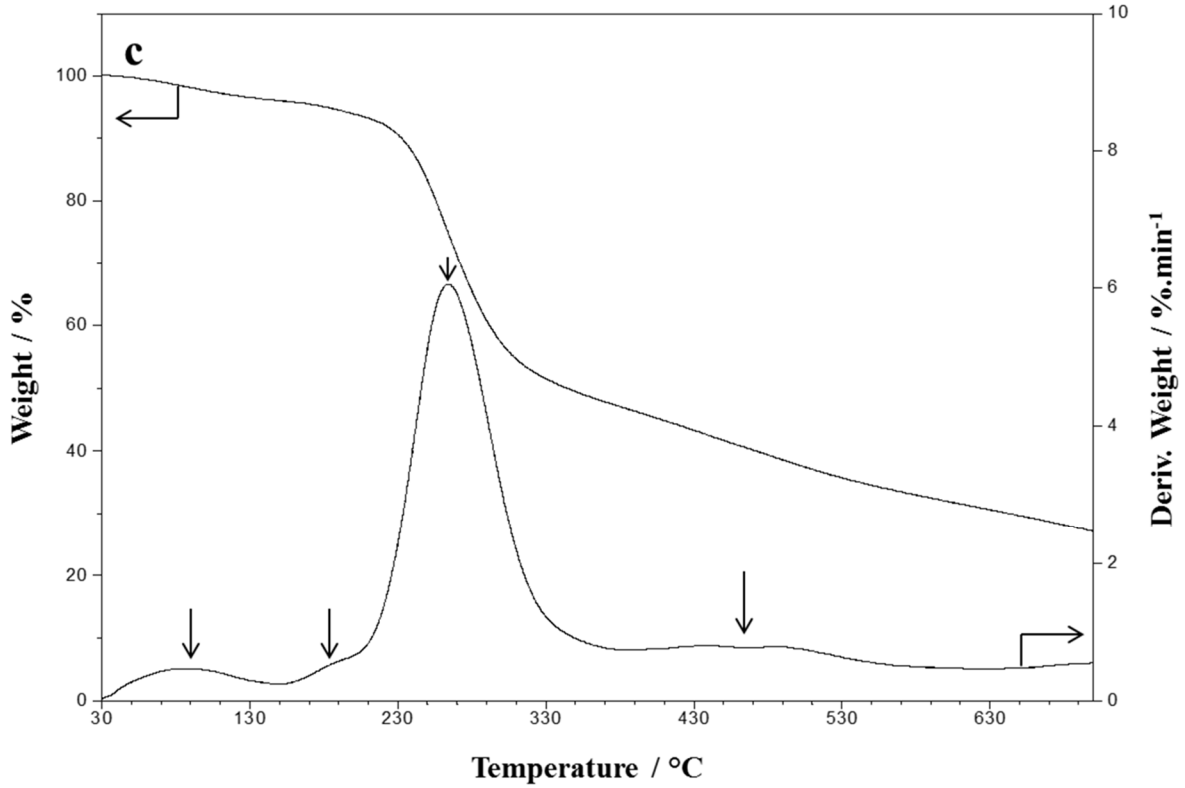

Fig. 3 4. a. 1D–WAXS of WSE; **b.** First and second scan DSC curves of WSE; **c.** TGA–DTG curves of WSE.

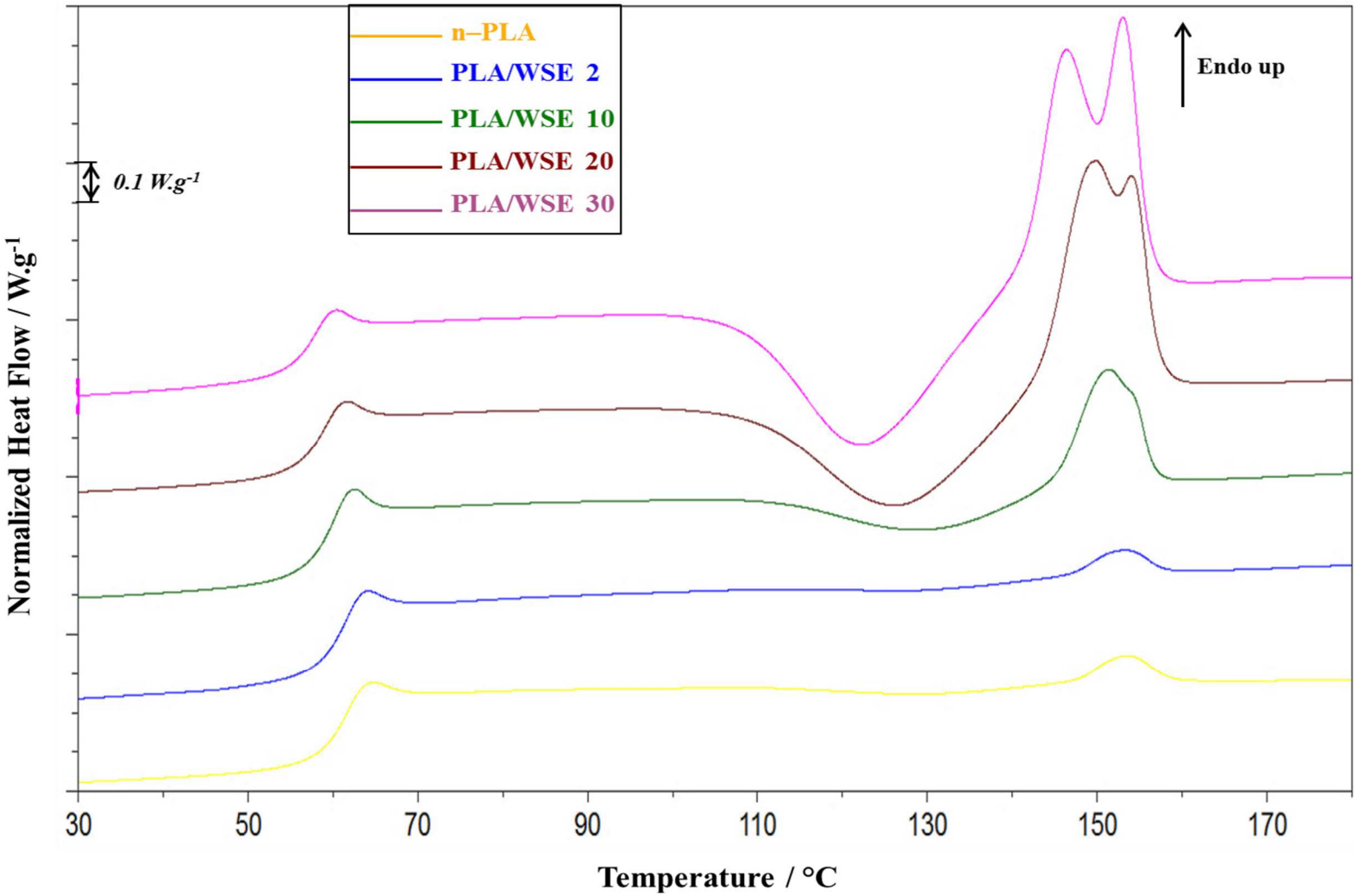

Fig. 4 5. Differential scanning calorimetry of n–PLA and PLA/WSE blends.

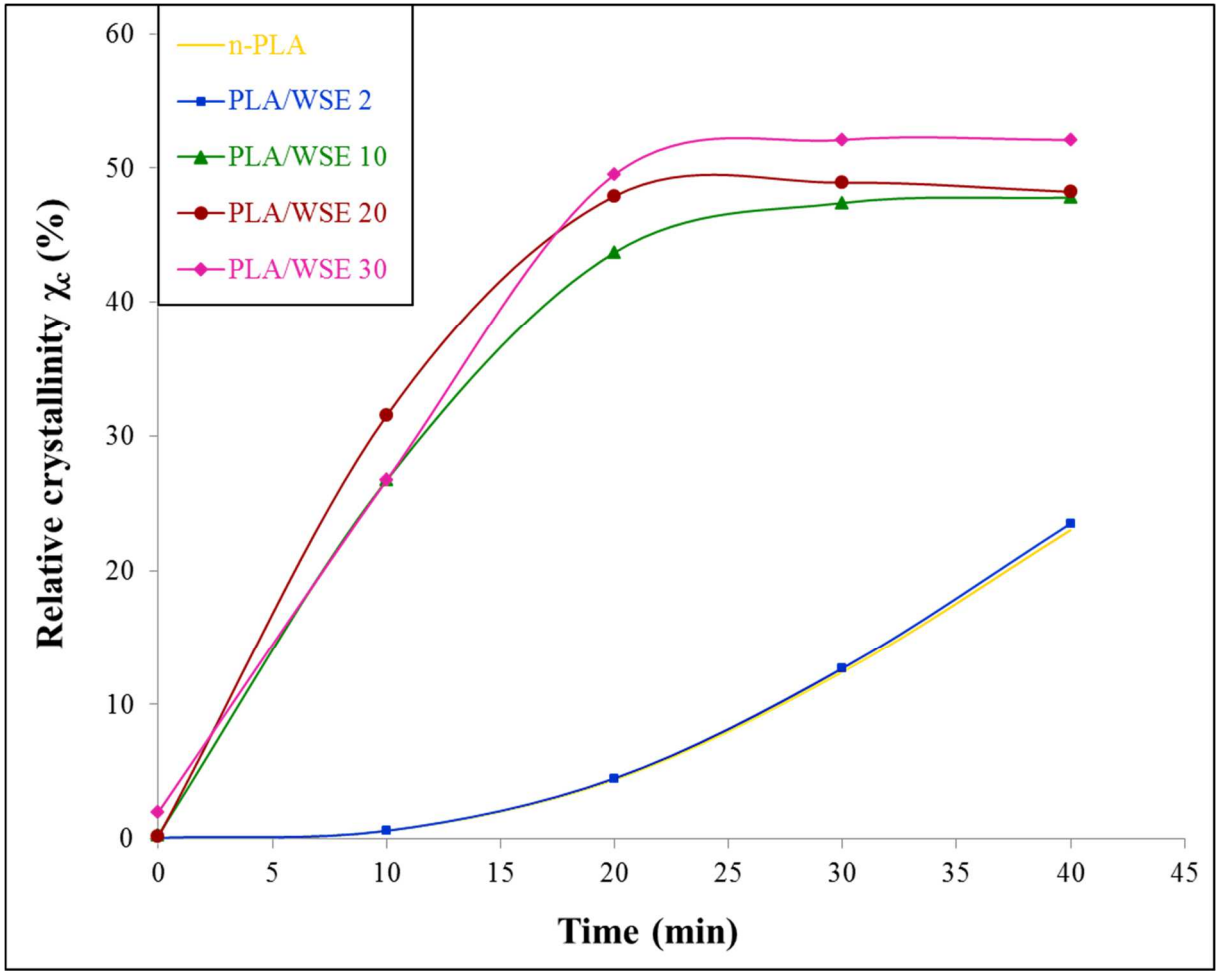

Fig. 5 ~~6~~. Crystallization kinetics of ~~PLA/WSE~~ PLA–based films at T_c = 120°C.

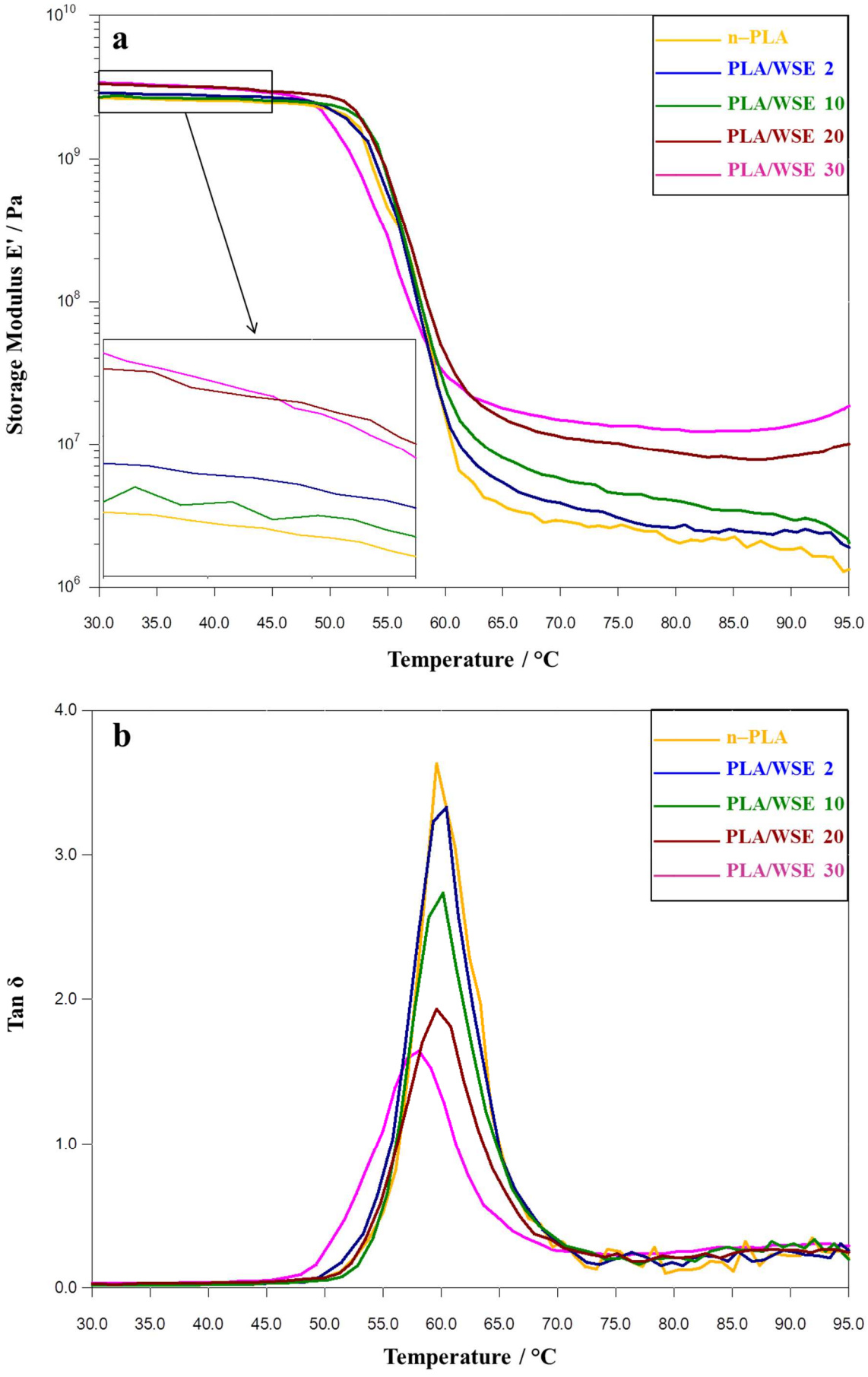

Fig. ~~7~~6. DMA thermograms of the **a.** *E' vs* temperature and **b.** tan δ *vs* temperature plots for PLA/WSE mixtures at various WSE content and n–PLA as reference.

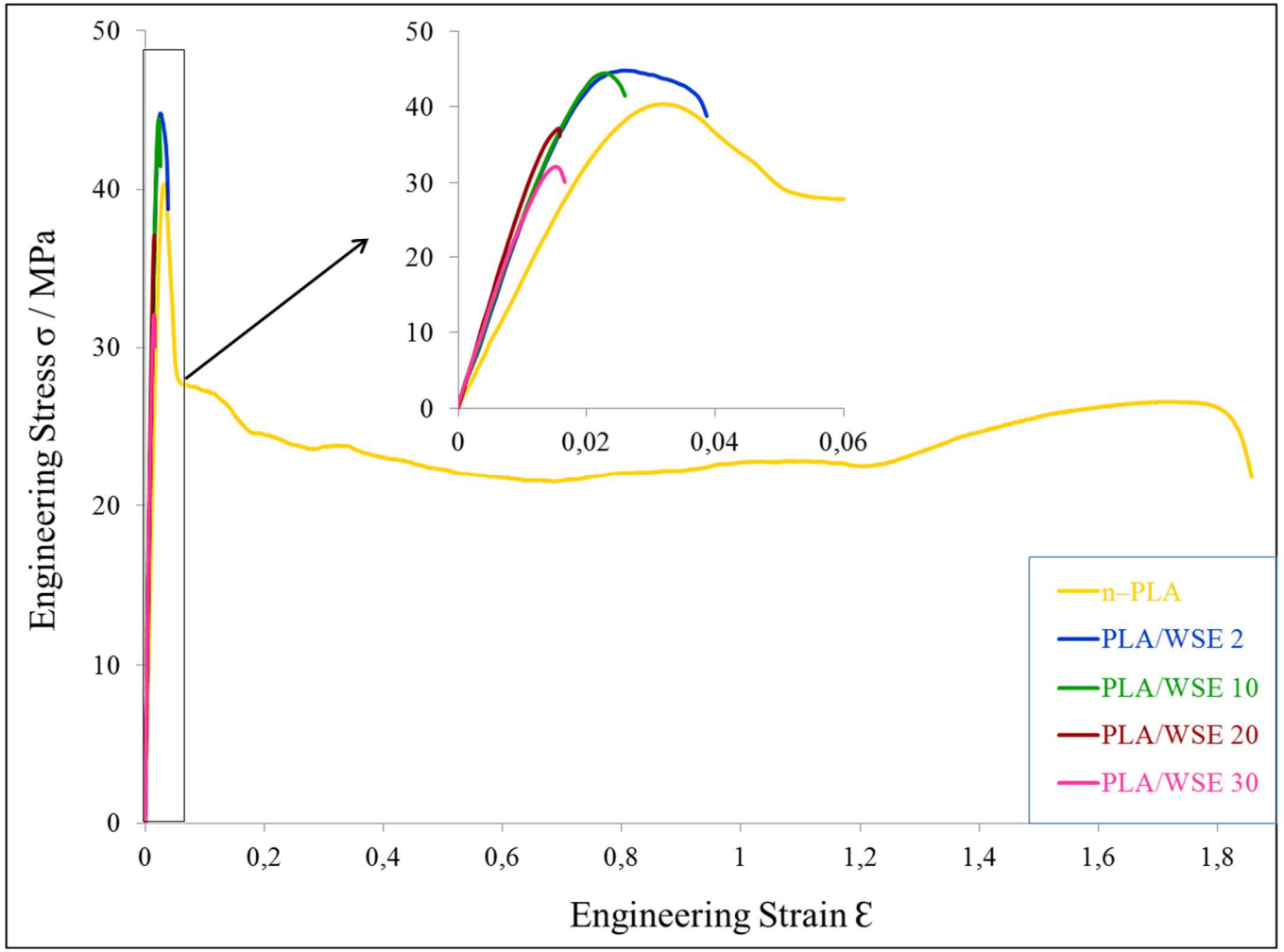

Fig. 87. Nominal stress–strain curves of n–PLA and PLA/WSE films T_d = 40°C; $\dot{\varepsilon}$ = 0,01s^{-1}.

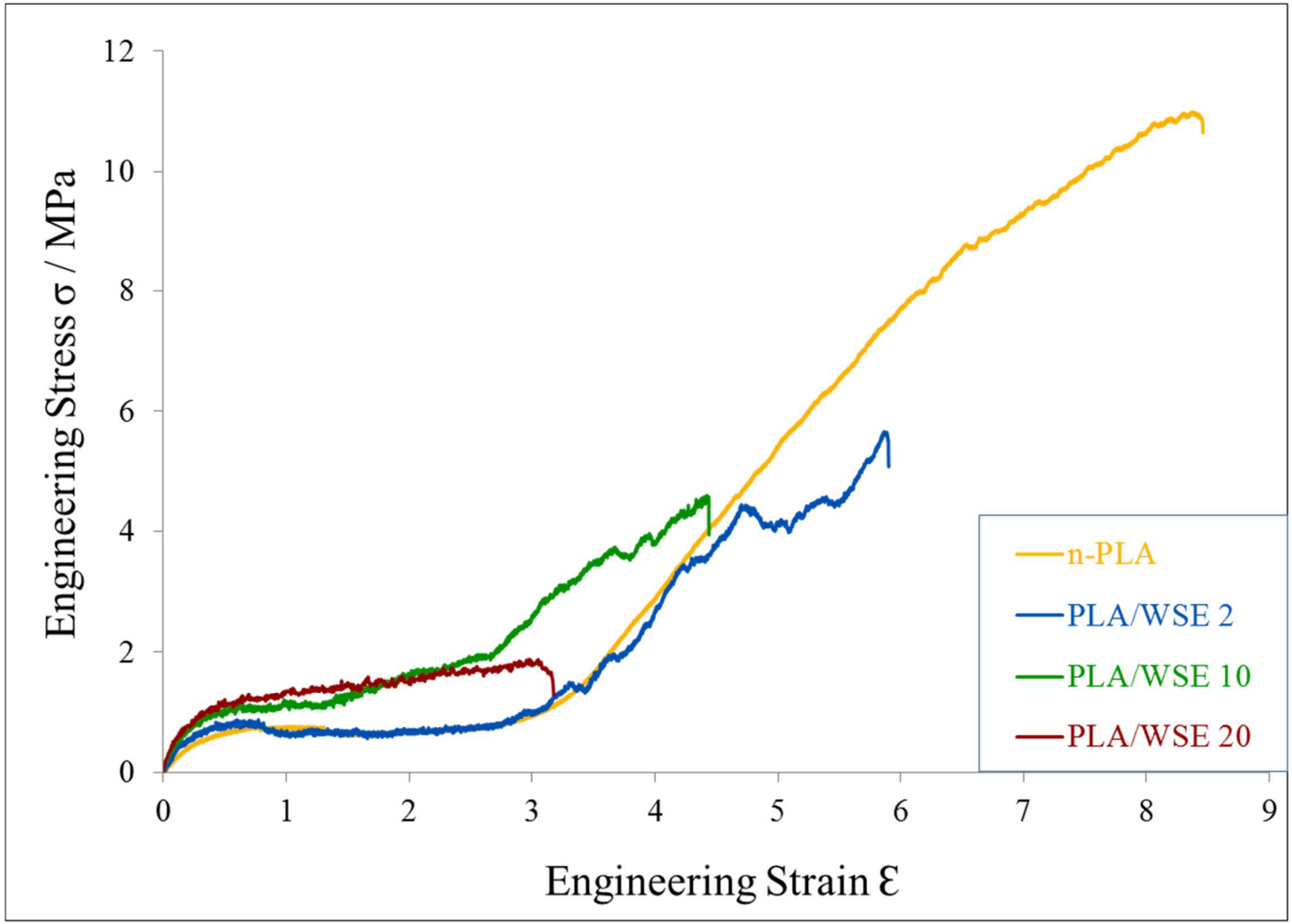

Fig. ~~9~~8. Nominal stress–strain curves of n–PLA and PLA/WSE films T=75°C; $\dot{\varepsilon}$=0,01s^{-1}.

PLA

+

WSE

1. Casting in $CHCl_3$

2. Thermocompression